J|A|C|S ARTICLES

Published on Web 07/27/2009

Unprecedentedly High Selective Adsorption of Gas Mixtures in *rho* Zeolite-like Metal−Organic Framework: A Molecular Simulation Study

Ravichandar Babarao and Jianwen Jiang*

Department of Chemical and Biomolecular Engineering, National University of Singapore, Singapore 117576

Received February 10, 2009; E-mail: chejj@nus.edu.sg

Ⓦ **This paper contains enhanced objects available on the Internet at http://pubs.acs.org/jacs.**

Abstract: We report a molecular simulation study for the separation of industrially important gas mixtures (CO_2/H_2, CO_2/CH_4, and CO_2/N_2) in *rho* zeolite-like metal-organic framework (*rho*-ZMOF). *Rho*-ZMOF contains a wide-open anionic framework and charge-balancing extraframework Na^+ ions. Two types of binding sites for Na^+ ions are identified in the framework. Site I is in the single eight-membered ring, whereas site II is in the α-cage. Na^+ ions at site I have a stronger affinity for the framework and thus a smaller mobility. The binding sites in *rho*-ZMOF resemble those in its inorganic counterpart *rho*-zeolite. CO_2 is adsorbed predominantly over other gases because of its strong electrostatic interactions with the charged framework and the presence of Na^+ ions acting as additional adsorption sites. At ambient temperature and pressure, the CO_2 selectivities are 1800 for the CO_2/H_2 mixture, 80 for the CO_2/CH_4 mixture, and 500 for the CO_2/N_2 mixture. Compared with other MOFs and nanoporous materials reported to date, *rho*-ZMOF exhibits unprecedentedly high selective adsorption for these gas mixtures. This work represents the first simulation study to characterize extraframework ions and examine gas separation in a charged ZMOF. The simulation results reveal that *rho*-ZMOF is a promising candidate for the separation of syngas, natural gas, and flue gas.

I. Introduction

In chemical industry, the separation of CO_2 from mixtures such as syngas, natural gas, and flue gas is tremendously important. Syngas is produced through steam−methane reformation and composed primarily of H_2 and CO_2. To purify the H_2, which is regarded as an ideal energy carrier and pollution-free fuel, CO_2 separation from syngas is a prerequisite.[1] Natural gas is an alternative substitute for environmentally unfriendly fossil fuels. Impurities such as CO_2 in natural gas must be removed for the improvement of calorie content.[2] A vast amount of flue gas is emitted by power plants, and a pressing issue in environmental protection is the need to sequester the greenhouse gas CO_2. Prior to sequestration, however, CO_2 must be separated from the flue gas.[3]

Techniques proposed to separate CO_2 from gas mixtures include amine absorption, cryogenic distillation, adsorption, and enzymatic conversion. Among these, adsorption in porous materials is energetically efficient and economically competitive. In past years, a number of experimental and simulation studies have been reported for the adsorptive separation of CO_2/H_2, CO_2/CH_4, and CO_2/N_2 mixtures in a variety of nanoporous materials such as carbons, zeolites, and emerging metal−organic frameworks (MOFs). In regard to removal of CO_2 from syngas, for example, separation of CO_2/H_2 mixtures in silicalite and ETS-10 (Engelhard TitanoSilicate No. 10) was studied, and a larger selectivity for CO_2 over H_2 was found in ETS-10.[4] A CO_2/H_2 mixture in a microporous silica was simulated, and the CO_2 selectivity was compared with experimental data.[5] Activated carbons mimicked by slit pores were investigated by simulation for CO_2/H_2 separation, and the CO_2 selectivity reached a maximum of 90 but decreased monotonically with increasing pore size.[6] In a dehydrated Na-4A zeolite, the CO_2 selectivity for CO_2/H_2 and CO_2/N_2 mixtures was predicted to decrease with increasing pressure at room temperature.[7] A simulation study for syngas in IRMOF-1 and Cu-BTC showed that the separation efficiency was affected by geometry, pore size, and electrostatic interactions.[8]

In connection with natural gas purification, the separation of CO_2/CH_4 mixtures was simulated in MFI with intersecting channels, in CHA and DDR with cages connected by narrow windows,[9,10] and in IRMOF-1 and Cu-BTC.[11] Adsorption of

(1) Hufton, J. R.; Mayorga, S.; Sircar, S. *AIChE J.* **1999**, *45*, 248.
(2) Singh, D.; Croiset, E.; Douglas, P. L.; Douglas, M. A. *Energy Convers. Manage.* **2003**, *44*, 3073.
(3) Noble, R. D.; Agrawal, R. *Ind. Eng. Chem. Res.* **2005**, *44*, 2887.
(4) Gallo, M.; Nenoff, T. M.; Mitchell, M. C. *Fluid Phase Equilib.* **2006**, *247*, 135.
(5) Richard, V.; Favre, E.; Tondeur, D.; Nijmeijer, A. *Chem. Eng. J.* **2001**, *84*, 593.
(6) Cao, D. P.; Wu, J. Z. *Carbon* **2005**, *43*, 1364.
(7) Akten, E. D.; Siriwardane, R.; Sholl, D. S. *Energy Fuels* **2003**, *17*, 977.
(8) Yang, Q. Y.; Zhong, C. L. *J. Phys. Chem. B* **2006**, *110*, 17776.
(9) Krishna, R.; van Baten, J. M.; Garcia-Perez, E.; Calero, S. *Chem. Phys. Lett.* **2006**, *429*, 219.
(10) Krishna, R.; van Baten, J. M.; Garcia-Perez, E.; Calero, S. *Ind. Eng. Chem. Res.* **2007**, *46*, 2974.
(11) Krishna, R.; van Baten, J. M. *Chem. Eng. Sci.* **2008**, *63*, 3120.

CO_2 and CH_4 in three types of nanostructures, namely, IRMOF-1, silicalite, and nanoporous carbon, were investigated. IRMOF-1 was found to have the largest capacity for adsorption of CO_2 and CH_4 but to be unsatisfactory for separation.[12] Atomistic simulations were reported for separation of CO_2/CH_4 and other mixtures in IRMOF-1; mixture effects were found to play a crucial role in determining the performance.[13,14] CO_2/CH_4 mixtures in carborane-based MOFs were studied, and a higher selectivity was reported in MOFs possessing exposed metal sites.[15] Mixed-ligand MOFs were examined for separation of CO_2 from CH_4, where mixture adsorption was predicted from the ideal-adsorption-solution theory and subsequently verified by simulation.[16] A simulation study of the separation of CO_2/CH_4 and CO_2/N_2 mixtures in IRMOF-1 and Cu-BTC reported that a higher selectivity was observed in Cu-BTC.[17]

Numerous studies of the separation of CO_2 from flue gas have also been reported. Adsorption of CO_2, CH_4, N_2, and their mixtures was measured in activated carbon Norit R1 at room temperature using a volume-gravimetric method.[18] CO_2 and N_2, as single components and as a binary mixture, were simulated in three zeolites with identical chemical composition but different pore structures.[19] The effects of various operating conditions on CO_2/N_2 separation in MFI and FAU membranes were investigated.[20,21] Other zeolites, such as mordenite, faujasite, and chabazite, were also examined for CO_2/N_2 separation.[20] A multiscale approach from quantum mechanics to molecular simulation was employed to study CO_2/N_2 separation in a nanoporous carbon (C_{168} schwarzite) and in comparison with cation-exchanged ZSM-5.[22] A simulation study was reported for separation of CO_2 from a $CO_2/N_2/O_2$ mixture in Cu-BTC, and the selectivity was ~35.[23] From fixed-bed adsorption, the separation of CO_2/N_2 was examined experimentally in microporous MOF-508b.[24]

To achieve high-efficiency separation of gas mixtures, the selection of an ideal adsorbent is critical. MOFs have emerged as an important class of hybrid inorganic−organic materials.[25] Remarkably different from zeolitic and carbonaceous structures, the controllable organic linkers and the variation of metal oxides in MOFs allow their pore size, volume, and functionality to be tailored in a rational manner. MOFs are considered as promising candidates for gas storage and separation. However, the reported selectivities for gas mixtures to date are not sufficiently high for practical applications. Recently, a unique subset of MOFs, zeolite-like MOFs (ZMOFs) have been developed.[26−31] They are topologically relevant to inorganic zeolites and exhibit similar structural properties. The substitution of oxygen atoms in zeolites by organic linkers leads to extra-large cavities and pores. This edge expansion approach offers great potential for the design and synthesis of very open materials. A number of ZMOFs contain charged frameworks and charge-balancing extraframework ions; an example is *rho*-ZMOF synthesized by the assembly of tetrahedral building units with a long ditopic organic linker.[26] The presence of extraframework ions in the pores of molecular dimensions increases the interactions with guest molecules and consequently enhances the storage, separation, or ion-exchange capability. For example, the exchangeable ions in natural and synthetic zeolites were found to play a key role in CO_2 adsorption.[32] Li- and Ca-exchanged faujasites are practically used in air separation by a pressure-swing adsorption process,[33] and the Ba-exchanged form is used in the selective separation of aromatic molecules.[34]

To the best of our knowledge, all previous studies of gas separation in MOFs have been conducted exclusively in neutral frameworks. Only recently have we reported, for the first time, the separation of gas mixtures in a charged MOF, namely, *soc*-MOF with a cationic framework.[35,36] The selectivity was found to be exceptionally high in *soc*-MOF. In the present study, the separation of CO_2/H_2, CO_2/CH_4, and CO_2/N_2 mixtures is investigated in *rho*-ZMOF, which, intriguingly, possesses an anionic framework. The static and dynamic properties of extraframework Na^+ ions in *rho*-ZMOF are also examined in detail. While experimental measurements of the adsorption of pure gases is relatively straightforward, quantitative measurements for gas mixtures is challenging. In this regard, molecular simulations are useful for predicting the behavior of gas mixtures and provide microscopic insight into the underlying mechanisms involved.

In section II, the molecular models for *rho*-ZMOF, Na^+, CO_2, H_2, CH_4, and N_2 are described. Section III briefly introduces the simulation methods, which include Monte Carlo (MC) and molecular dynamics (MD) simulations using a canonical ensemble to characterize Na^+ ions and MC simulations using a grand canonical ensemble to predict the adsorption of gas mixtures. In section IV, the isosteric heats and Henry constants for pure gases (CO_2, CH_4, H_2 and N_2) are examined first. Next, the isotherms, selectivities, simulation snapshots, and density contours for gas mixtures (CO_2/H_2, CO_2/CH_4, and CO_2/N_2) are presented, and the predicted selectivities in *rho*-ZMOF are compared with reported data in many other nanomaterials. Finally, concluding remarks are summarized in section V.

(12) Babarao, R.; Hu, Z. Q.; Jiang, J. W.; Chempath, S.; Sandler, S. I. *Langmuir* **2007**, *23*, 659.
(13) Keskin, S.; Sholl, D. S. *J. Phys. Chem. C* **2007**, *111*, 14055.
(14) Keskin, S.; Sholl, D. S. *Ind. Eng. Chem. Res.* **2009**, *48*, 914.
(15) Bae, Y. S.; Farha, O. K.; Spokoyny, A. M.; Mirkin, C. A.; Hupp, J. T.; Snurr, R. Q. *Chem. Commun.* **2008**, 4135.
(16) Bae, Y. S.; Mulfort, K. L.; Frost, H.; Ryan, P.; Punnathanam, S.; Broadbelt, L. J.; Hupp, J. T.; Snurr, R. Q. *Langmuir* **2008**, *24*, 8592.
(17) Martin-Calvo, A.; Garcia-Perez, E.; Castillo, J. M.; Calero, S. *Phys. Chem. Chem. Phys.* **2008**, *10*, 7085.
(18) Dreisbach, F.; Staudt, R.; Keller, J. U. *Adsorption* **1999**, *5*, 215.
(19) Goj, A.; Sholl, D. S.; Akten, E. D.; Kohen, D. *J. Phys. Chem. B* **2002**, *106*, 8367.
(20) Bernal, M. P.; Coronas, J.; Menendez, M.; Santamaria, J. *AIChE J.* **2004**, *50*, 127.
(21) Seike, T.; Matsuda, M.; Miyake, M. *J. Mater. Chem.* **2002**, *12*, 366.
(22) Jiang, J. W.; Sandler, S. I. *J. Am. Chem. Soc.* **2005**, *127*, 11989.
(23) Yang, Q. Y.; Xue, C. Y.; Zhong, C. L.; Chen, J. F. *AIChE J.* **2007**, *53*, 2832.
(24) Bastin, L.; Barcia, P. S.; Hurtado, E. J.; Silva, J. A. C.; Rodrigues, A. E.; Chen, B. *J. Phys. Chem. C* **2008**, *112*, 1575.
(25) Eddaoudi, M.; Kim, J.; Rosi, N.; Vodak, D.; Wachter, J.; O'Keefe, M.; Yaghi, O. M. *Science* **2002**, *295*, 469.
(26) Liu, Y. L.; Kravtsov, V. C.; Larsen, R.; Eddaoudi, M. *Chem. Commun.* **2006**, 1488.
(27) Sava, D. F.; Kravtsov, V. C.; Nouar, F.; Wojtas, L.; Eubank, J. F.; Eddaoudi, M. *J. Am. Chem. Soc.* **2008**, *130*, 3768.
(28) Tian, Y. Q.; Zhao, Y. M.; Chen, Z. X.; Zhang, G. N.; Weng, L. H.; Zhao, D. Y. *Chem.—Eur. J.* **2007**, *13*, 4146.
(29) Fang, Q. R.; Zhu, G. S.; Xue, M.; Sun, J. Y.; Wei, Y.; Qiu, S. L.; Xu, R. R. *Angew. Chem., Int. Ed.* **2005**, *44*, 3845.
(30) Dinca, M.; Han, W. S.; Liu, Y.; Dailly, A.; Brown, C. M.; Long, J. R. *Angew. Chem., Int. Ed.* **2007**, *46*, 1419.
(31) Dinca, M.; Dailly, A.; Tsay, C.; Long, J. R. *Inorg. Chem.* **2008**, *47*, 11.
(32) Bonenfant, D.; Kharoune, M.; Niquette, P.; Mimeault, M.; Hausler, R. *Sci. Tech. Adv. Mater.* **2008**, *9*, 013007.
(33) Coe, C. G. U.S. Patent 5,813,815, 1992.
(34) Neuzil, R. W. U.S. Patent 3,558,561, 1971.
(35) Babarao, R.; Jiang, J. W.; Sandler, S. I. *Langmuir* **2009**, *25*, 5239.

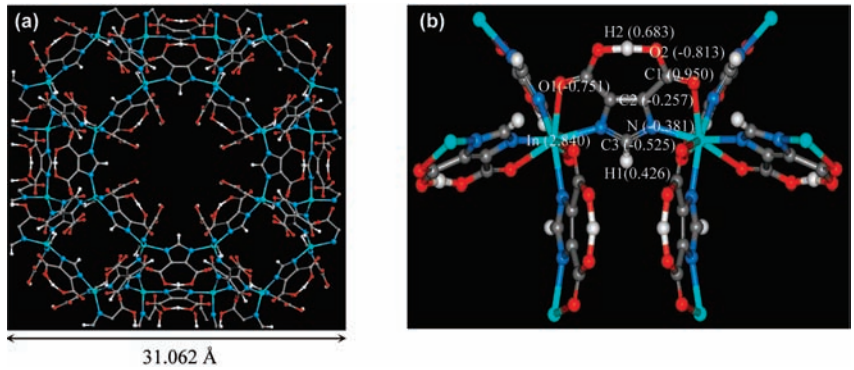

Figure 1. (a) Unit cell of *rho*-ZMOF. (b) Atomic charges in a fragmental cluster of *rho*-ZMOF calculated using DFT. The extraframework ions are not shown. Color code: In, cyan; N, blue; C, gray; O, red; H, white.

II. Molecular Models

Rho-ZMOF represents the first example of a four-connected MOF with a topology of *rho*-zeolite. It was synthesized by metal−ligand-directed assembly of In atoms and 4,5-imidazoledicarboxylic acid (H_3ImDC).[26] The space group of *rho*-ZMOF is $Im\bar{3}m$, and the lattice constants are $a = b = c = 31.062$ Å (Figure 1a). In the crystal structure, each In atom is coordinated to four N and four O atoms of four separate doubly deprotonated H_3ImDC (HImDC) to form an eight-coordinate dodecahedron. Each independent HImDC is coordinated to two In atoms, resulting in two rigid five-membered rings via N-, O-heterochelation. The structure has truncated cuboctahedra (α-cages) containing 48 In atoms, which link together through double eight-membered rings. The substitution of oxygens in *rho*-zeolite with HImDCs generates a very open framework with extra-large cavities that are 18.2 Å in diameter. Unlike *rho*-zeolite and other *rho*-aluminosilicates and aluminophosphates, *rho*-ZMOF contains twice as many positive charges (48 vs 24) per unit cell to neutralize the anionic framework. The elevated concentration of charge present in *rho*-ZMOF could augment ionic conductivity. In this work, the dehydrated *rho*-ZMOF is considered. Experimental thermogravimetric analysis showed that all residual water molecules could be completely evacuated.[26]

The atomic charges of *rho*-ZMOF framework atoms were calculated using density functional theory (DFT) on the basis of a fragmental cluster (Figure 1b). It has been widely recognized that quantum mechanically derived charges fluctuate appreciably when a small basis set is used; however, they tend to converge for basis sets beyond 6-31G(d). Consequently, in our DFT calculations, the 6-31G(d) basis set was used for all atoms except In, for which the LANL2DZ basis set was used. The DFT computations used the Lee−Yang−Parr correlation functional (B3LYP) and were carried out with the Gaussian 03 electronic structure package.[37] The concept of atomic charges is solely an approximation, and no unique straightforward method for rigorously determining atomic charges is currently available. In this study, the atomic charges were estimated by fitting to the electrostatic potential (ESP).[38] The extraframework Na^+ ions carried a positive unit charge. In addition to the Coulombic interactions, the dispersion interactions between framework atoms and Na^+ ions were represented by a Lennard-Jones (LJ) potential with parameters adopted from the universal force field (UFF).[39] The LJ cross-parameters were estimated by the Lorentz−Berthelot combining rules.[40] A number of simulation studies have shown that the UFF can accurately predict the adsorption and diffusion of gases in various MOFs.[12,41−45] For instance, good agreement between simulation and experiment was obtained for Ar adsorption in Cu-BTC.[41] The simulated isotherms and diffusivities of CO_2 and CH_4 in IRMOF-1 matched well with experimental data.[12,44,45]

CO_2 was represented as a three-site rigid molecule, and its intrinsic quadrupole moment was described by a partial-charge model.[46] The partial charges on the C and O atoms were $q_C = 0.576e$ and $q_O = -0.288e$ (where $e = 1.6022 \times 10^{-19}$ C is the elementary charge), respectively. The C−O bond length was 1.18 Å, and the O═C═O bond angle was 180°. The CO_2−CO_2 interaction was modeled as a combination of LJ and Coulombic potentials. H_2 was mimicked by a two-site model using LJ potential parameters fitted to the isosteric heat of H_2 adsorption on a graphite surface.[47] CH_4 was represented by a united-atom model interacting with the LJ potential. The potential parameters were adopted from the TraPPE force field, which was developed to reproduce the critical parameters and liquid densities of alkanes.[48] Similar to H_2, N_2 was also considered as a two-site model, with the LJ potential parameters fitted to the experimental bulk properties.[49] The electrostatic interaction between N_2 molecules was not considered, as it was found in our previous study that the incorporation of the quadrupole moment has an insignificant effect on N_2 adsorption.[22] Table 1 lists the potential parameters for Na^+ ion and the adsorbates.

(36) Jiang, J. W. *AIChE J.* **2009**, *55*, in press.
(37) Frisch, M. J.; et al. *Gaussian 03*, revision D.01; Gaussian, Inc.: Wallingford, CT, 2004.
(38) Besler, B. H.; Merz, K. M.; Kollman, P. A. *J. Comput. Chem.* **1990**, *11*, 431.
(39) Rappe, A. K.; Casewit, C. J.; Colwell, K. S.; Goddard, W. A.; Skiff, W. M. *J. Am. Chem. Soc.* **1992**, *114*, 10024.
(40) Maitland, G. C.; Rigby, M.; Smith, E. B.; Wakeham, W. A. *Intermolecular Forces*; Clarendon Press: Oxford, U.K., 1981.
(41) Vishnyakov, A.; Ravikovitch, P. I.; Neimark, A. V.; Bulow, M.; Wang, Q. M. *Nano Lett.* **2003**, *3*, 713.
(42) Garberoglio, G.; Skoulidas, A. I.; Johnson, J. K. *J. Phys. Chem. B* **2005**, *109*, 13094.
(43) Skoulidas, A. I.; Sholl, D. S. *J. Phys. Chem. B* **2005**, *109*, 15760.
(44) Babarao, R.; Jiang, J. W. *Langmuir* **2008**, *24*, 6270.
(45) Babarao, R.; Jiang, J. W. *Langmuir* **2008**, *24*, 5474.
(46) Hirotani, A.; Mizukami, K.; Miura, R.; Takaba, H.; Miya, T.; Fahmi, A.; Stirling, A.; Kubo, M.; Miyamoto, A. *Appl. Surf. Sci.* **1997**, *120*, 81.
(47) Cracknell, R. F. *Mol. Phys.* **2002**, *100*, 2079.
(48) Martin, M. G.; Siepmann, J. I. *J. Phys. Chem. B* **1998**, *102*, 2569.
(49) Murthy, C. S.; Singer, K.; Klein, M. L.; McDonald, I. R. *Mol. Phys.* **1980**, *41*, 1387.

Table 1. Force Field Parameters for Extraframework Ion and Adsorbates

species	site	σ (Å)	ε/k_B (K)	q (e)
Na^+	Na^+	2.658	15.09	+1
CO_2	C	2.789	29.66	+0.576
	O	3.011	82.96	−0.288
CH_4	CH_4	3.73	148.0	0
H_2	H	2.59	12.5	0
N_2	N	3.32	36.4	0

III. Simulation Methods

To characterize the locations of extraframework Na^+ ions in *rho*-ZMOF, MC simulations were carried out at 298 K using a canonical ensemble. The simulation box contained one unit cell of *rho*-ZMOF and 48 Na^+ ions, and periodic boundary conditions were applied in three dimensions. The unit cell was divided into three-dimensional grids, with the energy landscape tabulated in advance and then used by interpolation during simulation. In this way, the simulation was accelerated by 2 orders of magnitude. A spherical cutoff of 15.0 Å was used to evaluate the LJ interactions, and the usual long-range corrections were used beyond the cutoff. The use of the usual long-range corrections was an appropriate approximation because the error introduced by assuming homogeneity was small compared with the magnitude of the long-range corrections. For Coulombic interactions, a simple spherical truncation could result in significant errors; consequently, the Ewald sum with a tinfoil boundary condition was used. The real-space/reciprocal-space partition parameter and the cutoff for reciprocal lattice vectors were chosen to be 0.2 $Å^{-1}$ and 8, respectively, to ensure the convergence of the Ewald sum. These methods for calculating the LJ and Coulombic interactions were also used in the simulations described below. Initially, 48 Na^+ ions were introduced randomly into the system and followed by 10^7 trial moves. Two types of trial moves, displacement and regrowth, were used for Na^+ ions with equal probability. The acceptance criteria for the trial moves were based on the Metropolis algorithm.[50] After the MC simulations, the final configurations were used in the MD simulations to examine the mobility of Na^+ ions. The MD simulations were run for 3 ns, including 1 ns for equilibration and 2 ns for production, using the DL_POLY program.[51] The temperature was maintained at 298 K by the Nosé−Hoover thermostat. The potential and kinetic energies were monitored during the simulation to ensure equilibration. A time step of 1 fs was used for proper energy conservation, and the trajectory file was saved every 1 ps for analysis.

Before gas mixtures were examined, the adsorption of each pure gas (CO_2, CH_4, H_2, N_2) was studied in *rho*-ZMOF. Specifically, we calculated the isosteric heat and Henry constant at infinite dilution using MC simulations at 298 K. A single gas molecule was added into *rho*-ZMOF and subjected to three types of trial moves, namely, translation, rotation, and regrowth. The isosteric heat was evaluated by

$$Q_{st}^{\circ} = RT - \langle U_a^{\circ} \rangle \quad (1)$$

where R is the gas constant and $\langle U_a^{\circ} \rangle$ is the ensemble-averaged adsorption energy for a gas molecule with the adsorbent. The Henry constant K_H was evaluated using the expression

$$K_H = \beta \int \exp[-\beta u_a(\mathbf{r}, \omega)] \, d\mathbf{r} \, d\omega \quad (2)$$

in which $\beta = k_B T$ (where k_B is the Boltzmann constant) and $u_a(\mathbf{r}, \omega)$ is the adsorption energy for a gas molecule at position $\mathbf{r}$ with orientation ω. The integral yields the excess chemical potential of a single gas molecule upon adsorption. From the regrowth move, which is equivalent to the test-particle insertion method,[52] the excess chemical potential was evaluated.

Grand-canonical MC (GCMC) simulations were conducted for the adsorption of gas mixtures in *rho*-ZMOF at 298 K. Because the chemical potentials of the adsorbate in the adsorbed and bulk phases are identical at thermodynamic equilibrium, GCMC simulations allow one to relate the chemical potentials of the adsorbate in the two phases and thus have been widely used to simulate adsorption. The bulk composition was 50:50 for the CO_2/CH_4 mixture and 15:85 for both the CO_2/H_2 and CO_2/N_2 mixtures. The compositions chosen for these mixtures are ones typically found in practice in chemical industry. The framework was considered to be rigid during the simulations because adsorption involves low-energy equilibrium configurations and framework flexibility has a marginal effect on the adsorption of small gases. The number of trial moves in a typical simulation was 2×10^7, though additional trial moves were used at high loadings. The first 10^7 moves were used for equilibration and the subsequent 10^7 moves for ensemble averages. Six types of trial moves were randomly attempted in GCMC simulation: displacement, rotation, partial regrowth at a neighboring position, complete regrowth at a new position, swap with the reservoir, and exchange of molecular identity. The extraframework Na^+ ions were allowed to move during the simulation. As we shall observe, the positions of Na^+ ions were indeed shifted upon gas adsorption. To examine the effect of charged framework and extraframework Na^+ ions on separation, additional simulations were performed for gas mixtures in a neutral structure in which the charges on the framework and Na^+ ions were switched off.

IV. Results and Discussion

First, the extraframework Na^+ ions in *rho*-ZMOF are characterized in terms of static locations, radial distribution functions, and dynamic displacements. The locations are compared with those in the inorganic counterpart *rho*-zeolite. Next, the isosteric heats and Henry constants for pure CO_2, CH_4, H_2, and N_2 at infinite dilution are presented. Finally, the separations of syngas, natural gas, and flue gas in *rho*-ZMOF are reported. The adsorption isotherms, selectivities, density contours, and structural properties are specifically discussed in detail. The capability of *rho*-ZMOF for gas separation is compared with other MOFs and porous materials available in the literature.

Characterization of Na^+ ions. On the basis of the coordination environment and binding energy, two types of binding sites were identified for Na^+ ions in *rho*-ZMOF, as shown in Figure 2a. Site I is in the single eight-membered ring (S8MR) and at the entrance to the α-cage. Two neighboring S8MRs form a double eight-membered ring (D8MR). Site I is a distance of 5.0−5.3 Å from the nearest In atoms in the S8MR (Figure 2b) and ∼7.8 Å from the next-to-nearest In atoms in the D8MR (not shown). Site II is in the α-cage and proximal to the moiety of the organic linker. In one unit cell, 26 Na^+ ions are located at site I and the remaining ones at site II. Compared with site II, site I has a larger coordination number with neighboring atoms in the S8MR and thus a stronger interaction with framework. Intriguingly, these two types of binding sites in *rho*-ZMOF resemble those in its inorganic counterpart *rho*-zeolite.[53] In the latter, however, an additional type of site is located at the center of the D8MR and equally distanced from both S8MRs.

(50) Frenkel, D.; Smit, B. *Understanding Molecular Simulations: From Algorithms to Applications*, 2nd ed.; Academic Press: San Diego, CA, 2002.
(51) Smith, W.; Forester, T. R. *J. Mol. Graphics* **1996**, *14*, 136.
(52) Widom, B. *J. Chem. Phys.* **1963**, *39*, 2802.
(53) Lee, Y.; Reisner, B. A.; Hanson, J. C.; Jones, G. A.; Parise, J. B.; Corbin, D. R.; Toby, B. H.; Freitag, A.; Larese, J. Z. *J. Phys. Chem. B* **2001**, *105*, 7188.

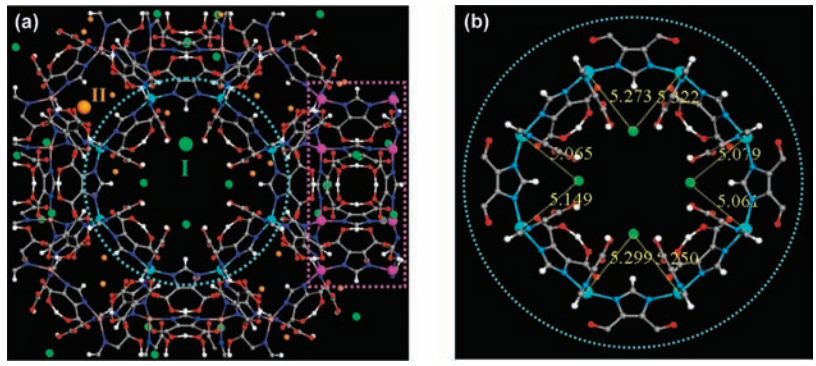

Figure 2. (a) Binding sites of Na^+ ions in *rho*-ZMOF. Site I (green) is in the single eight-membered ring (S8MR), while site II (orange) is in the α-cage. (b) Enlarged view of the central S8MR. Color code: In (S8MR), cyan; In (D8MR), pink; N, blue; C, gray; O, red; H, white.

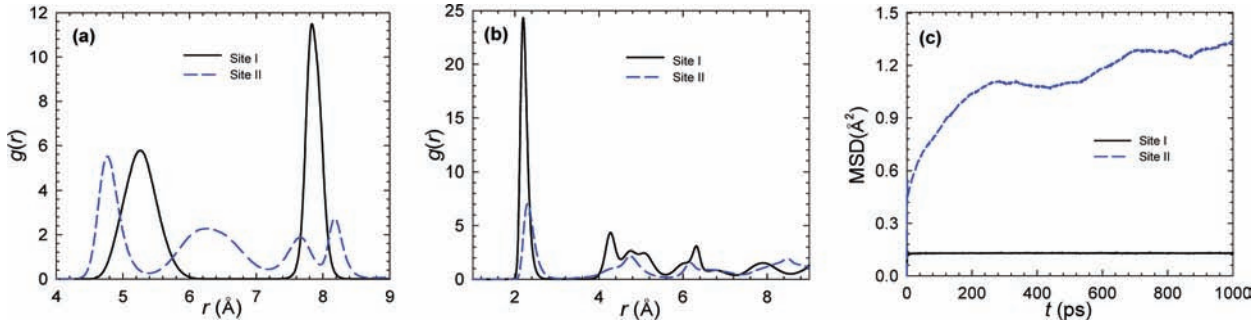

Figure 3. Radial distribution functions $g(r)$ between (a) Na^+ ions and indium atoms and (b) Na^+ ions and oxygen atoms. (c) Mean squared displacements of Na^+ ions.

To quantitatively identify the locations of the Na^+ ions, radial distribution functions $g_{ij}(r)$ were calculated as

$$g_{ij}(r) = \frac{\Delta N(r, r + \Delta r)V}{4\pi r^2 \Delta r N_i N_j} \quad (3)$$

where r is the distance between species i and j, $\Delta N(r, r + \Delta r)$ is the coordination number of j around i within a shell from r to $r + \Delta r$, V is the system volume, and N_i and N_j are the numbers of species i and j. Figure 3a shows $g(r)$ between Na^+ ions and In atoms of *rho*-ZMOF. At site I, $g(r)$ exhibits two distinct peaks at $r \approx 5.2$ and 7.8 Å. These are attributed to Na^+ ions around the nearest In atoms in the S8MR and the next-to-nearest In atoms in the D8MR, respectively. Na^+ ions at site I have a stronger affinity for the framework; consequently, the peak for site I is higher than that for site II. Figure 3b shows $g(r)$ between Na^+ ions and oxygen (O2) atoms of *rho*-ZMOF. A pronounced peak is observed at $r \approx 2.1$ Å, which indicates that Na^+ ions are located very close to the carboxylic groups because of the strong electrostatic attractions. Na^+ ions at site II have a smaller peak in $g(r)$ than those at site I, implying a relatively scattered distribution of Na^+ ions at site II.

The mobility of Na^+ ions was examined using mean-squared displacements (MSDs). The MSD was estimated from MD simulation as

$$\mathrm{MSD}(t) = \frac{1}{N}\sum_{i=1}^{N} |\Delta \mathbf{r}_i(t)|^2 \quad (4)$$

where t is time, N is the number of ions, and $\Delta \mathbf{r}_i(t)$ is the displacement of ion i from its initial position. Figure 3c shows the MSDs of Na^+ ions at sites I and II as functions of time. The MSD curve for site I is nearly flat with a negligible value of 0.15 Å^2. In contrast, the MSD at site II initially increases and then approaches a constant value of ~1.3 Å^2. The mobility of Na^+ is greater at site II than at site I because of the relatively weaker interaction with framework and the larger void space available around site II. Movies showing the motion of extraframework Na^+ ions in the (001) plane and (111) plane, as obtained from the MD simulations, are available. In general, the mobility of extraframework ions in *rho*-ZMOF is small. This could be attributed to the fact that degenerate favorable sites are far away from each other, which largely prohibits ion hopping from one site to other. In addition, steric hindrance due to the metal atoms and organic linkers also reduces the ion mobility. Consequently, the dynamics of extraframework ions can be regarded as local vibrations at their favorable binding sites.

Table 2. Isosteric Heats and Henry Constants for CO_2, CH_4, H_2, and N_2 in *rho*-ZMOF

species	Q_{st}° (kJ/mol)	K_H (mmol/g/kPa)
CO_2	58.25	50.37
CH_4	20.73	0.0133
H_2	6.02	0.0003
N_2	15.18	0.0026

Pure Gases. The strength of the interaction between adsorbate and adsorbent is directly reflected by the isosteric heat Q_{st}° and Henry constant K_H at infinite dilution. As listed in Table 2, CO_2 exhibits significantly larger Q_{st}° and K_H values than other gases. This is due to the extremely strong electrostatic interactions of quadrupolar CO_2 molecules with the highly charged framework and the concentrated Na^+ ions in *rho*-ZMOF. In silicalite, carbon, and neutral MOFs, Q_{st}° for CO_2 is in the range 13−33 kJ/mol and K_H is in the range 0.004−0.5 mmol cm^{-3}

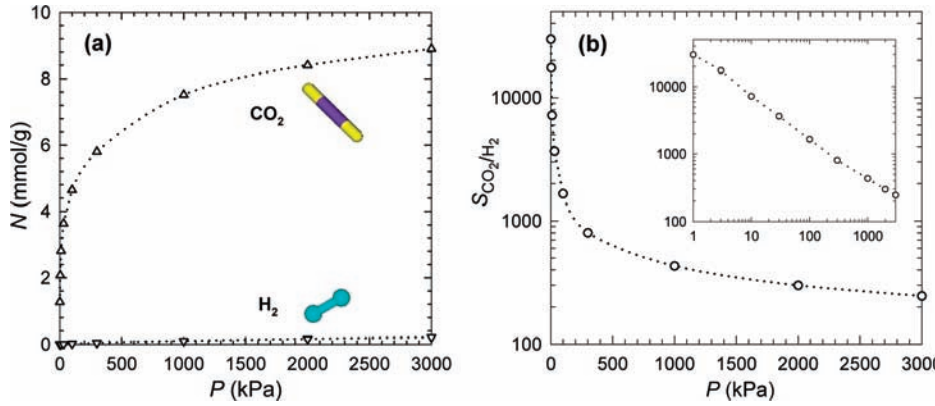

Figure 4. (a) Adsorption isotherm and (b) selectivity for a 15:85 CO_2/H_2 mixture.

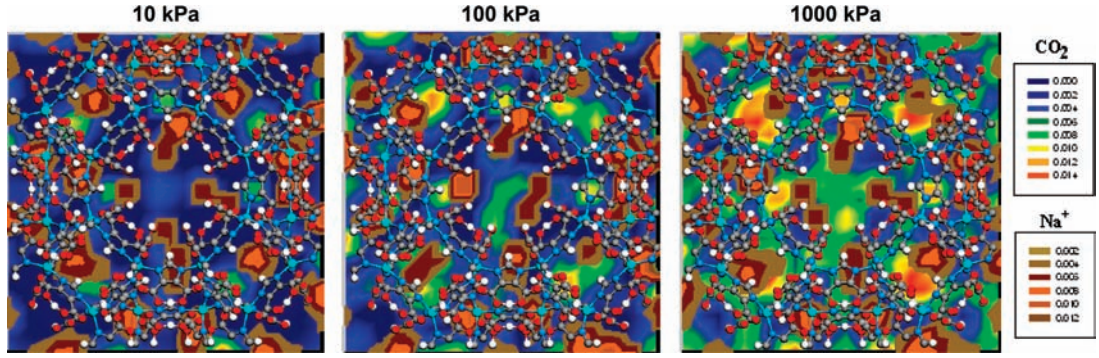

Figure 5. Density distribution contours of CO_2 molecules and Na^+ ions for a 15:85 CO_2/H_2 mixture at (left) 10, (center) 100, and (right) 1000 kPa.

kPa^{-1},[12,22,44,54] which are substantially smaller than the corresponding values in *rho*-ZMOF. The predicted Q_{st}° of CO_2 in *rho*-ZMOF is comparable to the experimentally measured Q_{st}° values in Na-ZSM5 (50 kJ/mol)[55] and Na-MOR (65 kJ/mol).[56] For CH_4, N_2, and H_2, the predicted Q_{st}° and K_H in *rho*-ZMOF are close to measured and simulated values in various nanostructures.[12,22,23,57] Among the four gases, H_2 has the smallest Q_{st}° and K_H, indicating the weakest affinity for *rho*-ZMOF.

CO_2/H_2 Mixture. Figure 4a shows the adsorption isotherm for a CO_2/H_2 mixture (bulk composition 15:85). A separate simulation in a larger box with $2 \times 2 \times 2$ unit cells gave very similar results (within statistical error), implying a negligible finite-size effect. The isotherm belongs to type I (Langmuirian), the characteristic feature of adsorption in microporous adsorbents. Over the entire range of pressure, CO_2 is more predominantly adsorbed than H_2 for three reasons. First, CO_2 is a three-site molecule and has a much stronger interaction with the framework than H_2 does. Second, the temperature of 298 K considered here is subcritical for CO_2 ($T_c = 304.4$ K) but supercritical for H_2 ($T_c = 33.2$ K); that is, CO_2 is more condensable than H_2 at 298 K. It has been observed in many studies that H_2 adsorption at room temperature is quite small in various MOFs, though the adsorption could be rather high at cryogenic temperatures.[58,59] Third, the highly ionic framework and the presence of extraframework ions induce strong electrostatic interactions with the quadrupolar CO_2 molecules, thereby enhancing CO_2 adsorption.

The separation of the CO_2/H_2 mixture is quantified by the selectivity $S_{ij} = (x_i/x_j)(y_j/y_i)$, where x_i and y_i are the mole fractions of component i in adsorbed and bulk phases, respectively. Figure 4b shows the selectivity S_{CO_2/H_2} for the CO_2/H_2 mixture in *rho*-ZMOF. At infinite dilution, the selectivity is equal to $K_H(CO_2)/K_H(H_2) \approx 1.6 \times 10^5$. With increasing pressure, it decreases sharply as a consequence of two factors. First, the adsorption sites in *rho*-ZMOF are heterogeneous, and adsorbate molecules occupy less favorable sites at higher pressures. Second, H_2 is much smaller than CO_2 and can pack into the partially filled pores more easily with increasing pressure. Under typical operating conditions (298 K and 1 atm) in pressure-swing adsorption, the selectivity is ~1800. Separation of CO_2 from syngas has been studied in other porous materials by both experiments and simulations. For example, the selectivity is 5 in MFI and 3.5 in ETS-10 for an equimolar CO_2/H_2 mixture.[4] In an activated carbon, the selectivity range is 60−90 for CO_2/H_2 mixtures with different mole fractions.[6] In zeolite Na-4A, the selectivity is 70 for a mixture with 98.6% H_2 and 1.4% CO_2.[7] The selectivity is 40 in IRMOF-1 and 150 in Cu-BTC at 298 K and 1 atm.[8] In charged *soc*-MOF, the selectivity is in the range 300−600.[36] In this study, the selectivity in *rho*-ZMOF is 1.6×10^5 at infinite dilution and 1800 under ambient conditions, the *highest* of all the values reported to date.

Figure 5 shows density distribution contours of CO_2 molecules and Na^+ ions for the CO_2/H_2 mixture in *rho*-ZMOF at

(54) Dunne, J. A.; Mariwals, R.; Rao, M.; Sircar, S.; Gorte, R. J.; Myers, A. L. *Langmuir* **1996**, *12*, 5888.
(55) Dunne, J. A.; Rao, M.; Sircar, S.; Gorte, R. J.; Myers, A. L. *Langmuir* **1996**, *12*, 5896.
(56) Delgado, J. A.; Uguina, M. A.; Gomez, J. M.; Ortega, L. *Sep. Purif. Technol.* **2006**, *48*, 223.
(57) Schmitz, B.; Muller, U.; Trukhan, N.; Schubert, M.; Ferey, G.; Hirscher, M. *ChemPhysChem* **2008**, *9*, 2181.
(58) Ryan, P.; Broadbelt, L. J.; Snurr, R. Q. *Chem. Commun.* **2008**, 4132.
(59) Kaye, S. S.; Dailly, A.; Yaghi, O. M.; Long, J. R. *J. Am. Chem. Soc.* **2007**, *129*, 14176.

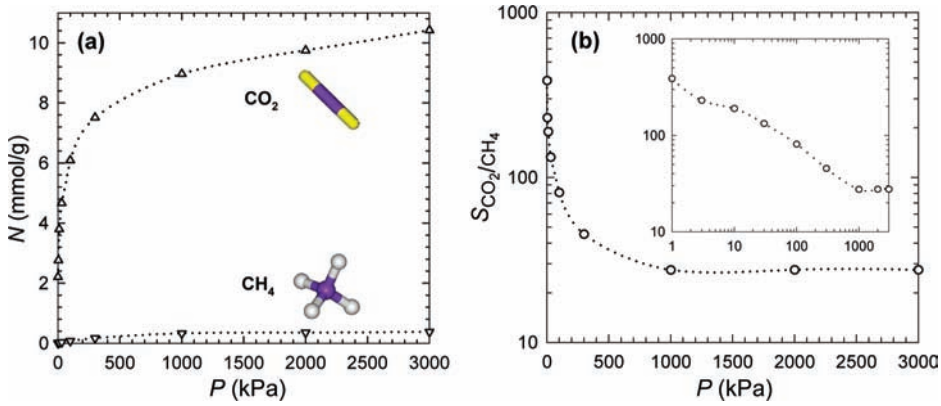

Figure 6. (a) Adsorption isotherm and (b) selectivity for a 50:50 CO_2/CH_4 mixture.

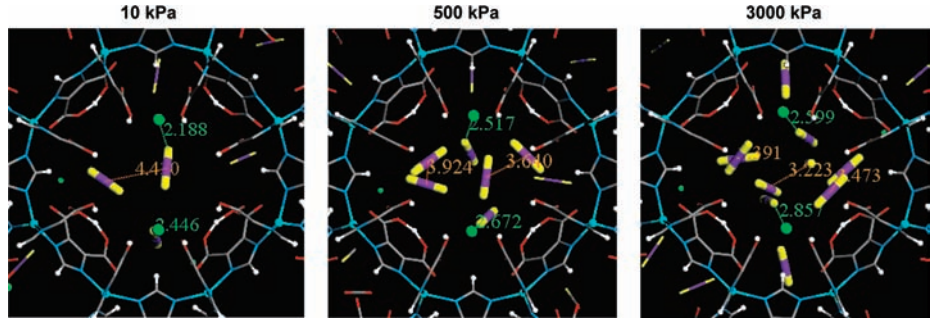

Figure 7. Locations of CO_2 molecules in the S8MR for a 50:50 CO_2/CH_4 mixture at 10, 500, and 3000 kPa. Na^+ ions and CO_2 molecules are represented by ball-and-stick structures. The $C_{CO_2}-C_{CO_2}$ (orange) and $Na^+-O_{CO_2}$ (green) distances are in angstroms.

10, 100, and 1000 kPa. At low and moderate pressures (10 and 100 kPa), CO_2 molecules are adsorbed near Na^+ ions. Therefore, the Na^+ ions act as additional sites for CO_2 adsorption because of the strong electrostatic interactions. At high pressure (1000 kPa), Na^+ ions are solvated by surrounding CO_2, and the void space between Na^+ ions is also occupied by CO_2. This suggests that additional adsorbed CO_2 molecules have relatively weaker interactions with the Na^+ ions. Interestingly, the locations of the Na^+ ions are observed to shift to some extent upon adsorption at different pressures.

Adsorption of the CO_2/H_2 mixture was also simulated in a neutral structure by switching off the charges of the framework and Na^+ ions. The isotherm and selectivity in the neutral structure are presented in Figure S1 in the Supporting Information. Compared with the results in Figure 4a, CO_2 adsorption in the neutral structure decreases by a factor of 3 at high pressures, whereas H_2 adsorption increases by a factor of 2. With increasing pressure, the selectivity in the neutral structure exhibits a trend similar to Figure 4b. However, at low pressures it decreases 3−1 orders of magnitude relative to that in the charged framework, and there is a less drastic decrease at high pressures. This clearly demonstrates the important role of the charged framework and Na^+ ions in the selective adsorption of CO_2 over H_2.

CO_2/CH_4 Mixture. Figure 6 shows the adsorption isotherm and selectivity for a CO_2/CH_4 mixture (bulk composition 50:50) in *rho*-ZMOF. As observed in Figure 4a for the CO_2/H_2 mixture, CO_2 adsorption is dominant. The selectivity is $K_H(CO_2)/K_H(CH_4) \approx 3800$ at infinite dilution and decreases to 80 at 1 atm. The selectivity in *rho*-ZMOF is the *highest* reported to date in MOFs and substantially higher than those in IRMOF-1 (2−3),[8,12,17] Cu-BTC (6−9),[8,17,35] carborane-based MOFs (17),[15] mixed-ligand MOFs (30),[16] and MOF-508b (3−6).[24] At pressures less than 5 atm, the selectivity in *rho*-ZMOF is also higher than that in *soc*-MOF.[35]

It is instructive to note that the selectivity of a gas mixture might be different in various MOFs and needs to be analyzed on a case-by-case basis. In our recent study of a CO_2/CH_4 mixture in *soc*-MOF, the selectivity increased with pressure and reached a plateau.[35] The increase was caused by the strong interactions of CO_2 molecules with the multiple binding sites and by the cooperative interactions of adsorbed CO_2 molecules. However, the selectivity for the CO_2/CH_4 mixture in *rho*-ZMOF decreases monotonically with increasing pressure. As further discussed below, this is a consequence of the significant reduction in the electrostatic interactions between CO_2 and *rho*-ZMOF with increased loading. The different behavior of the selectivity in *soc*-MOF and *rho*-ZMOF is attributed to the different framework topologies and charge densities. More specifically, there exist carcerand-like capsules and narrow channels with widths of ~10 Å in *soc*-MOF, whereas *rho*-ZMOF has a very open framework with large cavities with diameters of 18.2 Å. A unit cell of *soc*-MOF contains 8 NO_3^- ions, corresponding to a charge density of 7.1×10^{-4} e/Å^3. In contrast, *rho*-ZMOF possesses 48 Na^+ ions in a unit cell and a charge density of 1.6×10^{-3} e/Å^3. Therefore, the geometry constraints and surface interactions differ in the two charged MOFs, leading to different behavior for the selectivity versus pressure. Figure S2 in the Supporting Information shows the selectivity for the CO_2/CH_4 mixture in the neutral structure. Again, the charges on framework and extraframework ions play a key role in selective adsorption and separation. Compared with the values in Figure 6b, the selectivity decreases 3−1 orders of magnitude and exhibits qualitatively different behavior. With increasing pressure, the selectivity initially decreases and then increases. The initial decrease is attributed to the heterogeneous

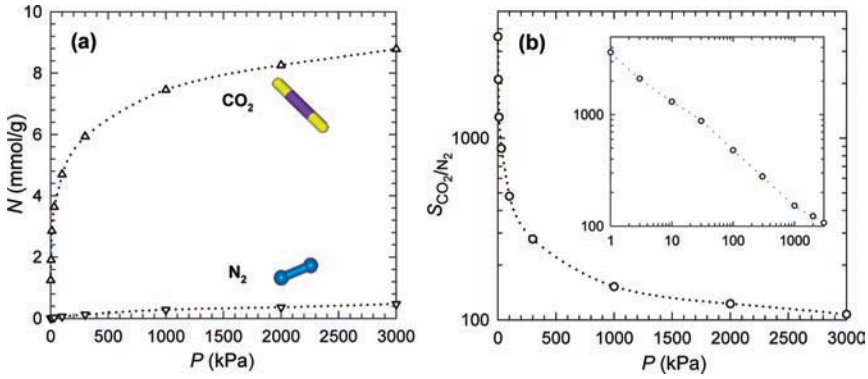

Figure 8. (a) Adsorption isotherm and (b) selectivity for a 15:85 CO_2/N_2 mixture.

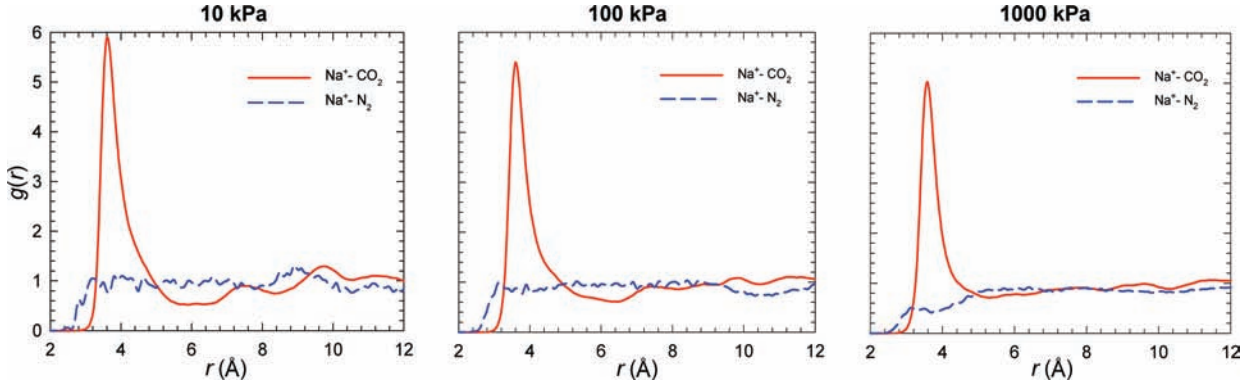

Figure 9. Radial distribution functions $g(r)$ between Na^+ ions and adsorbates for a 15:85 CO_2/N_2 mixture at (left) 10, (center) 100, and (right) 1000 kPa.

distribution of adsorption sites, and the later increase is due to cooperative interactions between CO_2 molecules.

Figure 7 represents the typical locations of CO_2 molecules in the S8MR for the CO_2/CH_4 mixture at 10, 500, and 3000 kPa. At low pressure, individual CO_2 molecules are observed to bind preferentially with Na^+ ions. As for the CO_2/H_2 mixture, Na^+ ions act as additional adsorption sites for CO_2. With increasing pressure, Na^+ ions are coordinated by more CO_2 molecules, i.e., increasingly solvated by surrounding CO_2 molecules. The distance between CO_2 molecules ($C_{CO_2}-C_{CO_2}$) becomes shorter with increasing pressure, while the distance between Na^+ and CO_2 ($Na^+-O_{CO_2}$) remains more or less constant. This implies an enhancement in the cooperative interactions between CO_2 molecules. As the pressure rises, however, more CO_2 molecules are adsorbed in the α-cage (figures not shown), and the electrostatic interactions between CO_2 and Na^+ ions are significantly reduced. In comparison, the enhanced cooperative interactions of CO_2 molecules are negligible. As a result, the selectivity decreases monotonically with increasing pressure.

CO_2/N_2 Mixture. Figure 8 shows the adsorption isotherm and selectivity for a CO_2/N_2 mixture (bulk composition 15:85) in *rho*-ZMOF. The trend is similar to those for the CO_2/H_2 and CO_2/CH_4 mixtures discussed above. CO_2 is adsorbed preferentially over N_2, and the selectivity decreases monotonically with pressure. At infinite dilution, the selectivity is $K_H(CO_2)/K_H(N_2) \approx 1.9 \times 10^4$ and decreases to 500 under ambient conditions. As illustrated in Figure S3 in the Supporting Information, the selectivity in the neutral structure drops significantly relative to that in Figure 8b. CO_2/N_2 separation in other nanoporous materials has been investigated. The selectivities are ~18.8 in zeolite Na-4A,[7] 15.3 in activated carbon Norit R1,[18] 30 in silicalite,[19] 100 in ITQ-3,[19] 14 in MFI,[20] 20 in FAU,[21] 35 in Cu-BTC,[17,23] and 3−6 in MOF-508b.[24] In Na-ZSM-5, the selectivity ranges from 4000 to 200 depending on Si/Al ratio.[22] The simulated selectivity in *rho*-ZMOF is the *highest* reported to date in MOFs and also substantially higher than in other materials.

To explore the structural information for CO_2 and N_2 in *rho*-ZMOF, the radial distribution functions $g(r)$ between Na^+ ions and adsorbates at 10, 100, and 1000 kPa are shown in Figure 9. A pronounced peak in $g(r)$ for Na^+-CO_2 is observed at $r =$ 3.6 Å at all the three pressures, but no such peak exists for Na^+-N_2. This confirms that CO_2 interacts with Na^+ ions more strongly than does N_2 because of the large quadrupole moment. As the pressure is increased from 10 to 100 and then to 1000 kPa, the peak height in $g(r)$ for Na^+-CO_2 drops, whereas the coordination number of CO_2 molecules surrounding Na^+ ions increases (data not shown). This indicates that Na^+ ions are solvated by more CO_2 molecules.

V. Conclusions

We have characterized the extraframework Na^+ ions and examined the separation of CO_2/H_2, CO_2/CH_4, and CO_2/N_2 mixtures in novel *rho*-ZMOF. The current study is the first of this type for a charged ZMOF. With a topology similar to its inorganic counterpart, *rho*-ZMOF contains twice as many positive charges as well as extra-large cavities. Two types of binding sites were identified for Na^+ ions. Site I is in the single eight-membered ring, and site II is in the α-cage, largely similar to *rho*-zeolite. The mobility of Na^+ ions was estimated by mean-squared displacements. Because of their strong affinity for the charged framework, Na^+ ions essentially vibrate around the

binding sites, though ions have a slightly greater mobility at site II than at site I.

An ideal adsorbent for CO_2 separation from a gas mixture should have a maximized capacity for CO_2 and minimized capacities for other species. For CO_2/H_2, CO_2/CH_4, and CO_2/N_2 mixtures in *rho*-ZMOF, CO_2 is adsorbed preferentially over the other gases. This is attributed to the highly charged framework and the large density of extraframework Na^+ ions; both exert strong electrostatic interactions on the quadrapolar CO_2 molecules. Furthermore, Na^+ ions act as additional adsorption sites and augment the interactions with CO_2 molecules. At low pressures, CO_2 is adsorbed proximally to Na^+ ions. With increasing pressure, Na^+ ions are coordinated and solvated by CO_2 molecules. The locations of Na^+ ions are shifted slightly upon adsorption. The selectivities for CO_2 over H_2, CH_4, and N_2 are 1800, 80, and 500 at 298 K and 1 atm, the typical conditions for pressure swing adsorption. The predicted selectivities in *rho*-ZMOF are the highest reported to date among various MOFs and unprecedentedly higher than those for other porous materials. *Rho*-ZMOF turns out to be an extremely promising material for the separation of syngas, natural gas, and flue gas. Combined with our recent study in *soc*-MOF, this work leads to the conclusion that charged MOFs are generally well-suited for the separation of (quadru)polar/nonpolar gas mixtures.

Acknowledgment. This work was supported by the National University of Singapore and the Singapore National Research Foundation. We are grateful to Prof. Mohamed Eddaoudi and Prof. Yunling Liu for helpful discussions.

Supporting Information Available: Complete ref 37 and adsorption isotherms and selectivities for gas mixtures in a neutral structure obtained by switching off the charges on framework and extraframework ions. This material is available free of charge via the Internet at http://pubs.acs.org.

JA901061J